Buckling transitions of an elastic filament in a viscous stagnation point flow

Laura Guglielmini, Amit Kushwaha, Eric S. G. Shaqfeh, and Howard A. Stone

Citation: Physics of Fluids **24**, 123601 (2012); doi: 10.1063/1.4771606
View online: http://dx.doi.org/10.1063/1.4771606
View Table of Contents: http://scitation.aip.org/content/aip/journal/pof2/24/12?ver=pdfcov
Published by the AIP Publishing

PHYSICS OF FLUIDS **24**, 123601 (2012)

Buckling transitions of an elastic filament in a viscous stagnation point flow

Laura Guglielmini,[1,a)] Amit Kushwaha,[2] Eric S. G. Shaqfeh,[3] and Howard A. Stone[4]
[1]*Center for Turbulence Research, Stanford University, Stanford, California 94305, USA*
[2]*Department of Mechanical Engineering, Stanford University, Stanford, California 94305, USA*
[3]*Department of Chemical and Mechanical Engineering, Stanford University, Stanford, California 94305, USA*
[4]*Department of Mechanical and Aerospace Engineering, Princeton University, Princeton, New Jersey 08544, USA*

(Received 6 June 2012; accepted 17 November 2012; published online 20 December 2012)

The interplay of viscous and elastic stresses is relevant to a number of flow problems involving slender elastic fibers. These range from the swimming of microorganisms to the transport of pulp fibers in processing flow as well as from nanotube and nanocarpet applications to semi-flexible polymer behavior. In some applications, slender fibers are attached to walls where they experience externally applied flows. In this paper, we focus on the model problem of a wall mounted filament in a (compressive) extensional flow and characterize the flow-induced bending and buckling of the fiber. Using a combination of stability analysis and numerical simulations (with the latter based on a discretized beam model), we show that, for a critical value of the ratio between viscous and elastic forces, the filament is susceptible to bending and buckling instabilities at supercritical bifurcation points. © *2012 American Institute of Physics*. [http://dx.doi.org/10.1063/1.4771606]

I. INTRODUCTION

The interplay between viscous and elastic stresses is relevant to a large number of flow problems involving deformable bodies in flow; slender elastic fibers in a viscous flow field are an example. In particular, in the low-Reynolds-number regime, elastodynamics is critical to understand how microorganisms swim by wave propagation along an elastic flagellum[1] or by the motion of an elastic filament driven at its base.[2–4] Arrays of cilia perform a variety of functions in the human body by virtue of their rapid beating and the resulting flow generation; these include clearance of the protective surface liquid in the airways of the lungs,[5] establishment of left/right asymmetry in the developing embryo,[6,7] the transport of gametes and embryos in the reproductive tract.[8]

Recent experiments in curved microchannels have demonstrated the formation of biofilm streamers, which are filaments of bacteria and polymer that develop in the flow, at the middle plane of the channel, and are connected to the side walls right after each inner corner.[9] In particular, filaments were shown to form in a region of weak but continuous extensional flow due to the presence of a secondary vortical flow at the corner and to be more prominent for corners with smaller radii of curvature.[10]

Other interesting applications of elastodynamics involve the deformation and migration of flexible fibers freely suspended in a flow, which may give rise to oriented phases or network structures;[11] applications involve also the dynamics of nanocarpets, i.e., high-density collection of nanotubes, which can be employed for flow or force sensing or to produce super-hydrophobic substrates. In experiments employing suspensions of microscopic fibers, it has been shown that there

a)Electronic mail: lauragug@stanford.edu.

is a sharp transition from zero to positive first normal stresses as a consequence of the buckling induced in the fibers.[12]

We consider here the problem of an elastic slender filament immersed in a viscous fluid and tethered at a stagnation point. The filament is initially aligned with the compression axis of the flow and may buckle and undergo complex dynamics as a result of the interplay between external viscous forces and elastic forces in the filament. Buckling of elastic slender filaments has been discussed previously for the case of free filaments in shear flow[13] and in cellular flow,[14,15] and a bifurcation to shape instabilities has been shown due to compression by the flow. Baczynski *et al.*[16] discussed instead the buckling instability of a filament under compressive load in two dimensions and in the presence of thermal fluctuations. Related research has been dedicated to the study of filaments tethered to a surface[17] or held in the flow at one end.[18] Moreover, with reference to the particular flow configuration that we consider, Beck and Shaqfeh[19] studied the dynamics of long-chain polymer molecules tethered to a plane wall and subject to a stagnation point flow, with the polymer aligned with the elongation axis of the flow and initially coiled; conformational hysteresis of the chain was shown to occur between the coiled and the stretched states.

Here, we describe a model for an elastic inextensible filament in a viscous flow and discuss the linear stability of a fiber aligned initially with the compression axis of the extensional flow (in Sec. II). We then introduce the discretized bead-rod chain model (Sec. III) that is used to simulate the complete nonlinear problem. Results from the combined asymptotic/numerical analysis of the filament dynamics are presented in Sec. IV. Finally, in Sec. V we outline a weakly nonlinear stability approach, which enables us to identify the Landau equation for the evolution of small perturbations in the neighborhood of transition points.

II. CONTINUUM MODEL FOR AN ELASTIC FILAMENT

We consider a slender, inextensible, and elastic filament immersed in a viscous two-dimensional flow $\mathbf{U}^\infty(\mathbf{x})$ (see Figure 1). In particular, we analyze two velocity distributions: a linear extensional flow $\mathbf{U}^\infty = (x, -y)$ and the quadratic extensional flow that characterizes the region proximal to a wall stagnation point, $\mathbf{U}^\infty = (xy, -y^2/2)$,[19] where the velocity field is made dimensionless with the modulus of the velocity $|\mathbf{U}^\infty|$ and the coordinates (x, y) with the length of the filament L. In both cases, the filament is tethered at the origin (0, 0), where the velocity vanishes, and is initially aligned with the axis of compression of the flow $x = 0$.

We assume external forces, such as gravity, and Brownian forces to be negligible; inertial effects are also hypothesized to be small. Hence, the fluid motion is governed by the Stokes equation and the filament dynamics results from the balance of elastic and viscous forces only. Under these conditions, the filament is characterized by the aspect ratio R/L (where R and L are, respectively, the radius and the length of the filament), by the area moment of inertia I and by Young's modulus E. Let $\mathbf{x}(s, t)$ be the dimensionless position vector of the filament centerline in a Cartesian reference frame, where s is the filament arc length and t the dimensionless time. The viscous force per unit length exerted on the filament by the undisturbed velocity field $\mathbf{U}^\infty$ can be expressed via slender-body theory,[20] whereas filament forces consist of bending and tensile contributions and can be expressed via the Euler-Bernoulli equation. The dimensionless governing equation for the filament to leading order in slenderness is[13,18]

$$\frac{\eta}{2}(2\mathbf{I} - \mathbf{x}_s^T\mathbf{x}_s)\cdot(\mathbf{U}^\infty - \mathbf{x}_t) = \mathbf{x}_{ssss} - (T(s,t)\mathbf{x}_s)_s, \tag{1}$$

where $T(s, t)$ is the tension in the filament, subscripts denote partial derivatives, and η represents the ratio of the viscous forces to the elastic forces and characterizes the behavior of an elastic thread immersed in a viscous flow

$$\eta = \frac{4\pi\mu L^3|U^\infty|}{EI\ln(L/R)}. \tag{2}$$

Note that we have used here as length scale the length of the filament L, as time scale the ratio $L/|\mathbf{U}^\infty|$ and as force scale the quantity EI/L^2. Furthermore, the constraint of inextensibility, expressed as $\mathbf{x}_s \cdot \mathbf{x}_s = 1$, provides a condition to be satisfied by the filament position $\mathbf{x}(s, t)$ at each instant.

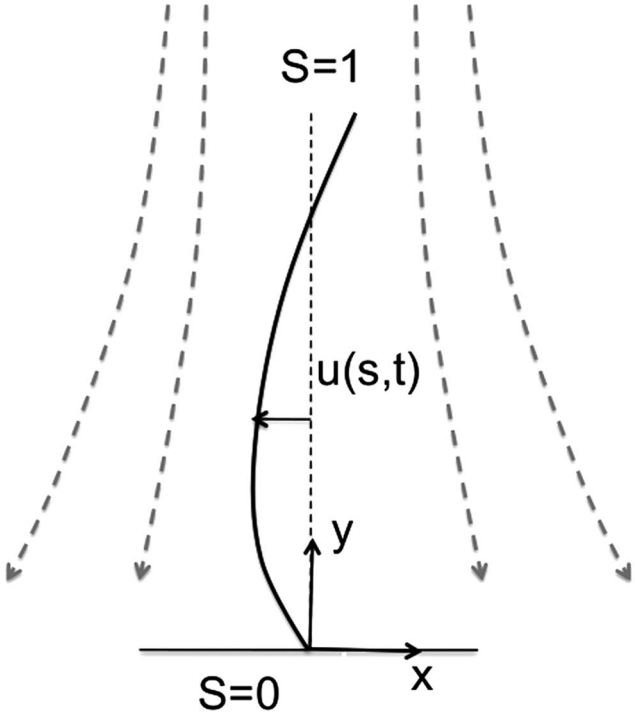

FIG. 1. A filament immersed in a viscous extensional flow, tethered at its base ($s = 0$) and initially aligned with the compression axis of the flow. The filament position is described by the vector $\mathbf{x}(s, t)$, with s a curvilinear coordinate running along its length. In the linearized problem, we describe the evolution of the filament in term of the displacement $u(s, t)$ orthogonal to the axis $x = 0$. Here, s has been scaled by the length of the inextensible filament, so the end of the filament is at $s = 1$.

As mentioned above, we consider a thread that is held at one end and free at the other end (see Figure 1). At the free end, position $s = 1$, we require zero force and zero torque, which can be expressed as $\mathbf{x}_{ss} = \mathbf{x}_{sss} = \mathbf{0}$ and $T(s = 1) = 0$. At the fixed end, position $s = 0$, the filament can be either clamped, so that its position and slope are fixed, $\mathbf{x}(s = 0, t) = \mathbf{x}_s(s = 0, t) = \mathbf{0}$, or hinged, in which case only the position is fixed and zero torque is applied, i.e., $\mathbf{x}(s = 0, t) = \mathbf{x}_{ss}(s = 0, t) = \mathbf{0}$.

A. Linear theory

We study the linear stability of a filament held at the origin $\mathbf{x} = (0, 0)$, initially lying at the straight equilibrium position, and immersed in a planar extensional flow field, $\mathbf{U}^\infty = (x, -y)$ or $\mathbf{U}^\infty = (xy, -y^2/2)$. We follow the approach proposed by Becker and Shelley[13] for a buckling filament in a shear flow, where, for the flow geometry considered here, the unperturbed shape of the filament is not a function of time. The position of the filament is specified as $x_i = s\delta_{i2} + u(s, t)\delta_{i1}$, where the first term represents the unperturbed straight "base" state and $u(s, t)$ is a perturbation orthogonal to the compression axis of the flow. Moreover, the velocity field is evaluated at the filament position $U_i^\infty = U_i^\infty(x_i)$.

We linearize Eq. (1) for small deflections $|u| \ll 1$ for the two velocity distributions $\mathbf{U}^\infty$. For the linear extensional flow $\mathbf{U}^\infty = (x, -y)$, the component along x_2 of the linearized Eq. (1) reduces to $T_s = \eta\, 2s$, which can be integrated to obtain, given the boundary condition $T(s = 1) = 0$, the tension distribution $T(s) = \eta(s^2 - 1)/4$. From the component in x_1 of the linearized Eq. (1), by accounting for the identified expressions for $T(s)$ and $T_s(s)$, we obtain an equation of evolution for the perturbation $u(s, t)$,

$$u_t = u + su_s + (s^2 - 1)\frac{u_{ss}}{4} - \frac{1}{\eta}u_{ssss}\,. \tag{3}$$

TABLE I. Values of η at which the modes associated with the eigenvalues with larger real part become unstable for a filament tethered at the stagnation point of an extensional flow. We also report critical values from literature[13,14] for a free filament in a shear flow and in an extensional flow. Notice that for an hinged filament an unstable mode, which describes rotation about the rod base, is present for any value of η.

	Free filament	Hinged filament	Clamped filament
Shear flow	$\eta_c = 153.2$ (Becker and Shelley[13])		
$(x, -y)$	$\eta_c = 153.2$ (Young and Shelley[14])	$\eta_{c2} = 48.4$	$\eta_{c1} = 5.25$
		$\eta_{c3} = 225.5$	$\eta_{c2} = 103.7$
$(xy, -y^2/2)$		$\eta_{c2} = 122.5$	$\eta_{c1} = 9.2$
		$\eta_{c3} = 585.$	$\eta_{c2} = 250.$

Analogously, for the quadratic extensional flow $\mathbf{U}^\infty = (xy, -y^2/2)$, we derive

$$T(s) = (s^3 - 1)\frac{\eta}{12} \quad \text{and} \quad u_t = su + \frac{s^2}{2}u_s + (s^3 - 1)\frac{u_{ss}}{12} - \frac{1}{\eta}u_{ssss}\,. \tag{4}$$

The equation for the perturbation $u(s, t)$ is completed by the boundary conditions $u_{ss} = u_{sss} = 0$ for $s = 1$ and either $u = u_s = 0$ (clamped filament) or $u = u_{ss} = 0$ (hinged filament) for $s = 0$.

We discuss the filament instability to in-plane disturbances of the form $u(s, t) = u(s)e^{\lambda t}$, subject to the appropriate boundary conditions. Pseudospectral collocation, using the Galerkin-type Chebyshev expansion $u(s) = \sum_{n=0}^{N} a_n \Phi_n(2s - 1)$ with Φ_n Chebyshev functions of the first kind, yields a generalized matrix eigenvalue problem for the mode amplitudes a_n with eigenvalue λ. The details depend on the compliance η, with stability when $\lambda < 0$ and instability for $\lambda > 0$. In Table I, we report the first two critical values of η_c, i.e., the values of η at which a normal mode becomes unstable, for the four combinations of flow field and boundary conditions considered. We observe that for a clamped filament a first unstable mode, which describes a "bending" response, appears for $\eta_{c1} = 5.25$ in the case of a linear extensional flow and for $\eta_{c1} = 9.2$ in the case of a quadratic extensional flow. A second mode describing a "buckling" response becomes unstable for $\eta_{c2} = 103.7$ and $\eta_{c2} = 250$, respectively for the two flow configurations. When the filament is hinged instead, a vanishing torque is applied at the base of the filament and an unstable mode describing "rotation" about the point (0, 0) is always present, even for vanishing values of η. For the hinged case we identify, and report in the table, the first two values of η at which further unstable modes, describing buckling, appear. For completeness, we also include in the table the critical effective compliance at which buckling occurs for the cases of a free filament in a shear flow[13] and in a linear extensional flow.[14]

III. NUMERICAL METHOD: A BEAD-ROD CHAIN MODEL

In order to verify the validity of our linear theory, we numerically solve the full nonlinear problem by employing the appropriate bead-rod chain model. The filament is represented as a bead-rod chain consisting of N beads connected by $N - 1$ rigid rods of length a (Figure 2). The beads serve as interaction points with the solvent, whereas the massless rods act as rigid constraints in the chain and keep every bead at a constant distance away from its neighboring beads. Since we are interested in the chain dynamics under flow and in proximity of a wall, it is appropriate to use a modified version of the Kramers freely jointed bead-rod chain model[21] that includes the bending modulus, i.e., the Kratky-Porod model.[22,23] In this model, the chain has more segments than Kuhn steps, so that it is possible to allow the bending modulus to control the persistence length regardless of the discretization of the chain.[24] The governing equations for the dynamics of the chain are obtained by summing the external forces acting on the beads

$$\mathbf{F}_i^H + \mathbf{F}_i^T + \mathbf{F}_i^C + \mathbf{F}_i^W + \mathbf{F}_i^B = \mathbf{0}, \qquad i = 1, 2, ..., N, \tag{5}$$

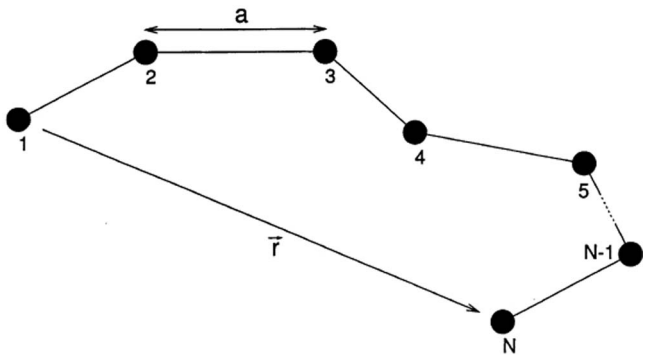

FIG. 2. Freely jointed bead-rod chain (Kramers chain), which models a polymer constituted by N beads and $N-1$ rods of length a.

where the subscript i refers to the bead number and $\mathbf{F}^H$, $\mathbf{F}^T$, $\mathbf{F}^C$, $\mathbf{F}^W$, $\mathbf{F}^B$ are, respectively, the hydrodynamic drag force, the constraint force, the bending force, the wall force, and the Brownian force. The hydrodynamic force is generally written as the drag acting on the individual bead in the absence of hydrodynamic interactions and fluid inertia. For this specific problem, we chose the drag coefficient as the non-isotropic leading order term for a cylindrical shape of aspect ratio $\epsilon = R/a \ll 1$ from slender-body theory,[20] so that we have

$$\mathbf{F}_i^H = -\frac{2\pi\mu a}{\log\epsilon^{-1}}(2\mathbf{I} - \mathbf{r}_{i,s}\mathbf{r}_{i,s}) \cdot (\dot{\mathbf{r}}_i - \mathbf{U}_i^\infty), \tag{6}$$

where $\dot{\mathbf{r}}_i$ is the velocity of the bead, $\mathbf{U}_i^\infty$ is the solvent velocity at the bead i position and $\mathbf{r}_{i,s}$ is a vector tangent to the chain at position i ($\mathbf{r}_{i,s} \approx \mathbf{r}_{i+1} - \mathbf{r}_i$). The constraint force keeps two neighboring beads at a constant distance a from each other, and can be written in terms of the tensions T_i in the rods as follows:

$$\mathbf{F}_i^T = T_i\mathbf{q}_i - T_{i-1}\mathbf{q}_{i-1}, \tag{7}$$

where $\mathbf{q}_i = (\mathbf{r}_{i+1} - \mathbf{r}_i)/a$ is the orientation of the rod i connecting beads i and $i+1$ at positions $\mathbf{r}_i$ and $\mathbf{r}_{i+1}$, respectively. The bending force is obtained by evaluating the first variation of the bending energy of a semi-flexible filament,[25]

$$\mathbf{F}_i^C = \hat{\ell}_p a k_B \mathcal{T} \kappa_{ss} \approx \frac{\hat{\ell}_p}{a} k_B \mathcal{T} \frac{(-\mathbf{r}_{i-2} + 4\mathbf{r}_{i-1} - 6\mathbf{r}_i + 4\mathbf{r}_{i+1} - \mathbf{r}_{i+2})}{a^2}, \tag{8}$$

where $\hat{\ell}_p$ is is the persistence length of the chain, $\mathcal{T}$ is the temperature, and κ the local curvature of the chain, which is discretized in terms of the bead positions $\mathbf{r}_i$. The wall exclusion force $\mathbf{F}_i^W$ is a non-physical interaction that prevents the beads from penetrating the wall, has direction perpendicular to the wall, is characterized by a constant dictating its strength and by a cutoff distance, i.e., the distance from the wall at which repulsion acts on the beads. We use the expression for the wall repulsive force that has been discussed in Hoda and Kumar[26] and accounts for the Lennard-Jones potential (see Appendix B). Finally, the Brownian force $\mathbf{F}_i^B$ represents the frequent collisions between the beads and the solvent molecules and is mathematically modeled as a quantity with zero mean and a second moment that balances the dissipative forces.[24]

After substitution of the different forces acting on the beads into Eq. (5) and rearranging, we obtain a set of equations governing the evolution of the position vectors $\mathbf{r}_i$[27]

$$d\mathbf{r}_i = \mathbf{U}_i^\infty + \mathbf{A} \cdot \left(\frac{\mathbf{F}_i^T + \mathbf{F}_i^C + \mathbf{F}_i^W}{\zeta}\right)dt + \sqrt{\frac{2k_B\mathcal{T}}{\zeta}}\mathbf{L} \cdot d\mathbf{W}_i, \tag{9}$$

where $i = 1, 2, .., N$, $\zeta = 2\pi\mu a/\log\epsilon^{-1}$ is the drag coefficient and $d\mathbf{W}_i$ is a Weiner process, i.e., a Gaussian random number with zero mean and variance dt. Moreover, we denote with $\mathbf{A}$ the inverse matrix of the non-isotropic portion of the drag force in Eq. (6), $\mathbf{A} = (\mathbf{I} + \mathbf{r}_{i,s}\mathbf{r}_{i,s})/2$, and with $\mathbf{L}$ the

Cholesky decomposition of $\mathbf{A}$, i.e., $\mathbf{L} \cdot \mathbf{L}^T = \mathbf{A}$. Further, the constraint that the separation between adjacent beads has to remain equal to a needs to be enforced. A system of $(2N - 1)$ equations for N position variables $\mathbf{r}_i$ and $(N - 1)$ tensions T_i is identified and solved with a predictor-corrector scheme for the position equation and LU factorization for the equation for the tension. For the case of the clamped filament, the boundary condition at the base of the filament is easily implemented by requiring $\mathbf{r_1} = (0, 0)$ and $\mathbf{r_2} = (0, 1)$, while for the hinged filament we impose $\mathbf{r_1} = (0, 0)$ and $\mathbf{r_2} = (4\mathbf{r_3} - \mathbf{r_4})/5$, which expresses the condition of zero torque and free rotation. Finally, we find that we can achieve a good precision on the tension distribution if we apply at the base of the filament, i.e., at position $\mathbf{r_1}$, an external force $\mathbf{F}_1^{\text{ext}} = \sum_i \mathbf{F}_i^H$.

In the final formulation of the governing equations, the distance between adjacent beads a serves as the length scale, the bead diffusion time $\zeta a^2/k_BT$ serves as the characteristic time scale, and the forces are made dimensionless with $k_B\mathcal{T}/a$. Two dimensionless parameters appear, namely, the dimensionless persistence length $\ell_p = \hat{\ell}_p/a$ and the Peclet number, defined as the ratio between the convective and the diffusive time scales, $Pe = \dot{\gamma}(\zeta a^2/k_B\mathcal{T})$, with ζ the drag coefficient and $\dot{\gamma}$ the shear rate, $\dot{\gamma} = |\mathbf{U}^\infty|/(a(N - 1))$.

IV. RESULTS

A. Filament dynamics

With reference to the bead-rod chain model introduced in Sec. III, we will consider the dynamics of an elastic filament in the limit of very large Peclet number, i.e. we will assume thermal fluctuations to be negligible. Under these conditions, the dynamics of the filament will depend only on the length of the filament N and on the ratio Pe/ℓ_p. We observe that, in the absence of thermal fluctuations, the bead-rod chain model is a discretized version of the continuum model described by Eq. (1), provided that the dimensionless groups that appear in the two are properly related. In fact, we see that we can directly write the effective compliance η as $\eta = 2\text{Pe}N(N - 1)^2/\ell_p$, where we have expressed the bending modulus in term of the persistence length, as $\hat{\ell}_p = EI/(k_BT)$. Moreover, all of the numerical solutions that will be described below have been validated via successive grid refinements, that is, by considering filaments of increasing numbers of beads until convergence is reached.

We first present a few typical solutions for a tethered elastic filament, initially aligned with the compression axis of the flow and freely evolving after a tiny disturbance with respect to its equilibrium position is introduced (see Figure 3). The various positions of the filament refer to various time instants during the transient, until the filament reaches its final equilibrium position. The filament is either immersed in a linear extensional flow, in Figures 3(a), 3(b), and 3(d), or in a quadratic extensional flow, in Figure 3(c); moreover, the filament can be clamped (Figures 3(a)–3(c)) or hinged (Figure 3(d)). For a clamped filament, its orientation at the base cannot change and we observe that its equilibrium shape at the end of the transient is more "bent" for larger values of η and thus smaller rigidity of the filament. For the case in Figure 3(a), the filament is characterized by a value of η smaller than the critical value for buckling, so that it progressively bends, while for the case in Figure 3(b) we have $\eta = 2000$ and the filament buckles with a dominant mode of high order. In Figure 3(c), the clamped filament is immersed in a quadratic extensional flow and its compliance η is not much larger than the critical value for buckling, so that the beam is modestly compressed along the vertical axis and progressively bent towards its equilibrium configuration. Finally, in Figure 3(d) the filament is hinged at the base, hence it is allowed to rotate and continuously does so until it is aligned with the flow along $y = 0$. We observe that, since its compliance is much larger than the critical value for buckling (see Table I), the filament buckles significantly and then, due to the action of the flow, it rotates about its base and aligns with the elongational axis of the flow.

From this brief discussion, we appreciate that a simple way to discern between a bending and buckling behavior of the beam is to examine the end-to-end length of filament, that is, the distance between the two ends of the chain. For a clamped filament in a linear extensional flow, we show in Figure 4 the evolution of the filament end-to-end length in time for values of the compliance η in the range $0 - 2000$ (η decreases for curves from left to right in the plot). Note that a dashed

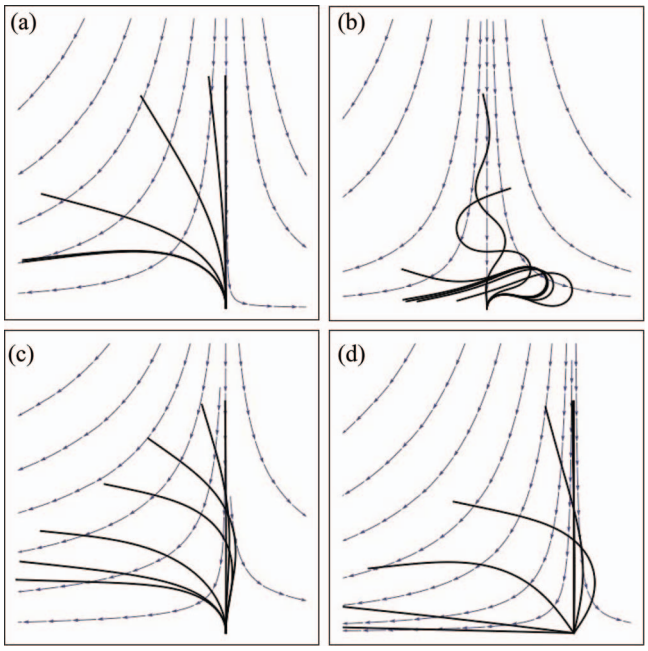

FIG. 3. Figures show the position of a tethered filament in a compressive extensional flow at successive time instants, until a stationary configuration is reached. A clamped filament in linear extensional flow for (a) $\eta = 50$, (b) $\eta = 2000$, (c) in a quadratic extensional flow for $\eta = 750$. (d) A hinged filament in a linear extensional flow for $\eta = 200$.

curve is used for $\eta = 50$, 100, for which the filament has "bending" behavior, while a continuous line is used for values of $\eta > \eta_{c2}$, corresponding to a "buckling" behavior. We observe that for a bending filament the end-to-end length is a monotonically decreasing function of time, while for a buckling filament the end-to-end length displays a point of minimum at a certain time. In fact, as shown in Figure 3, a buckling filament is initially compressed along the axis $x = 0$ and, at the same time, it starts to bend in the outward direction of the flow. The minimum in the end-to-end length occurs when the "buckling" mode is dominant over the "bending" mode. It is possible that, when the "buckling" phase is completed and before or while the filament is being rotated by the flow towards its equilibrium position, the free end gets close to the filament base and the end-to-end length is very small (see, for example, the curve for $\eta = 1000$). The curve to the extreme left of the plot describes the evolution of the end-to-end length of the filament for $\eta = 2000$, while the position

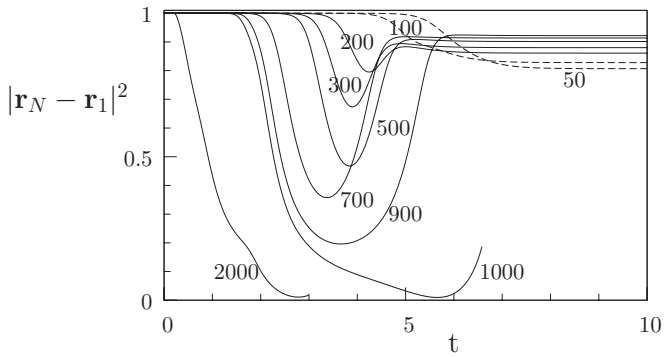

FIG. 4. End-to-end length of the filament, defined as $|\mathbf{r}_N - \mathbf{r}_i|$, versus time, for decreasing values of η and increasing values of the persistence length l_p (η decreases from left to right over the range $50 - 2000$), for the case of a clamped filament in a linear extensional flow. The dashed line is used for cases in which the filament exhibits bending only, while a continuous line is used for larger values of η, such that the filament buckles.

of the filament for this case is shown at various instants in Figure 3(b). The filament collapses on its base and reaches a metastable configuration characterized by a very small end-to-end length.

B. Unstable modes analysis

The linear analysis described in Sec. II A can provide not only the critical values of the compliance η, but also some useful insights into the filament dynamics. For a clamped filament in a wall stagnation point flow we show in Figure 5(a) the behavior of the first four eigenvalues for increasing values of the parameter η. The eigenvalue characterized by the largest real part is negative for very small η and changes sign at the first critical point $\eta_{c1} = 9.2$, when the filament becomes unstable to "bending." A second eigenvalue, which is associated with a buckling mode, becomes unstable at the critical value $\eta_{c2} = 250$. Insets show the unstable eigenfunctions for several values of η, where the color coding for the eigenfunctions allows to identify the corresponding eigenvalue at the various η, and continuous and dashed curves represent, respectively, the real and the imaginary part of complex eigenfunctions. We observe that as η increases the shape of the eigenfunctions changes, so that, for example, the first eigenfunction initially describes "bending," while for larger values of η a point of relative minimum appears in its shape (for $\eta = 270$) and it represents a "buckling" mode (a further point of maximum appears for $\eta = 900$). Also, the first unstable eigenvalue remains the eigenvalue with largest real part over the range of values of η considered. Finally, we observe that for a sufficiently large compliance η the first two eigenfunctions (and eigenvalues) get nearer in value until the eigenvalues and the corresponding eigenfunctions become complex ($\eta = 2060$), with the same real parts and conjugate imaginary parts. A second couple of complex conjugate eigenvalues and associated eigenfunctions appears for $\eta \approx 5200$. The case of a clamped filament in a linear flow presents very similar features, with the only difference being in the values of η at the critical points.

For the case of a hinged filament in a linear extensional flow, we plot in Figure 5(b) the evolution of the eigenvalues with largest real part as the compliance η is increased. As mentioned, the boundary condition at the base allows the filament to rotate, so that the filament is unconditionally unstable and an initial perturbation will always displace the rod away from the compression axis of the flow. Hence, a positive eigenvalue, associated with a "rotation" mode eigenvector (see inset), is present even for arbitrarily small η. For $\eta_{c2} = 48.4$ a further mode, describing a "buckled" shape, becomes unstable and for $\eta \approx 100$ dominates over the first mode. For $\eta_{c3} = 225.5$ a third eigenvalue, associated with a higher-order mode, becomes positive. Over the range $300 < \eta < 500$ a first couple of complex conjugate eigenvalues and associated complex conjugate eigenfunctions appear. We show in blue the imaginary part of the complex eigenvalues as a function of η, while in the insets the imaginary part of the associated complex eigenfunction is represented with a dashed line. For larger values of η more couples of complex conjugate eigenvalues appear over finite intervals of η.

For the sake of completeness, we show in Figure 5(c) analogous results for the case of a free filament in a linear extensional flow. We observe that, while for the free filament in extensional flow the eigenvalues diagram is characterized by alternating odd and even dominant modes as η is increased,[14] for our problem the boundary condition at the base selects the shape of the characteristic modes with respect to the center of the flow. Moreover, pairs of complex conjugate eigenvalues appear also for the free filament. We note that in this case, as for the case of a hinged filament, the most unstable eigenvalue is complex only for a small range of values of η, while for a clamped filament the most unstable mode is always complex for a large value of η.

C. Comparison with the linearized problem

An appropriate way to analyze results from numerical simulations is to expand the position of the filament $x_1(s, t)$ at each time in a basis formed by the eigenfunctions $\phi_i(s, \eta)$ of Eqs. (3) and (4) when associated with the two kinds of boundary conditions. We can in fact define $x_1(s, t) = \sum b_i(t)\phi_i(s, \eta)$, with $b_i(t) = \langle \phi_i^\dagger(s, \eta), x_1(s, t)\rangle / \langle \phi_i^\dagger(s, \eta), \phi_i(s, \eta)\rangle$, where $\phi_i^\dagger(s)$ are the eigenfunctions of the associated adjoint problem. Note that all the linearized problems considered

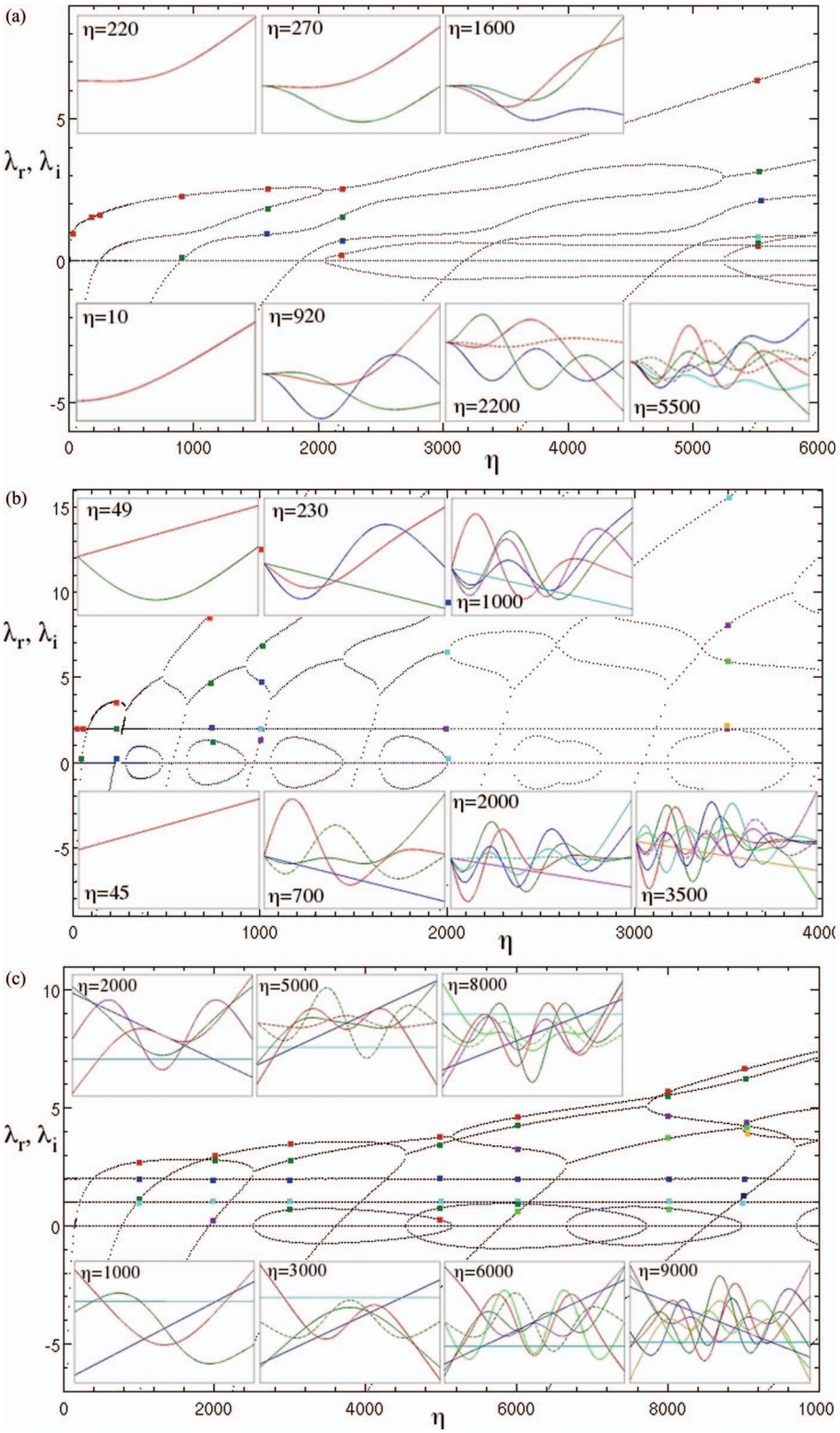

FIG. 5. Behavior of eigenvalues with larger real part versus η, (a) for a clamped filament in a wall stagnation point flow, (b) a hinged filament in a linear extensional flow, (c) a free filament in a linear extensional flow.[14] In black the real part and in blue the imaginary part of various eigenvalues. In inset, we report the shape of unstable eigenfunctions over the domain $s \in [0, 1]$ for various η. The color coding for the eigenfunctions allows to identify the corresponding eigenvalue at the various η, while continuous and dashed curves represent respectively the real and the imaginary part of complex eigenfunctions.

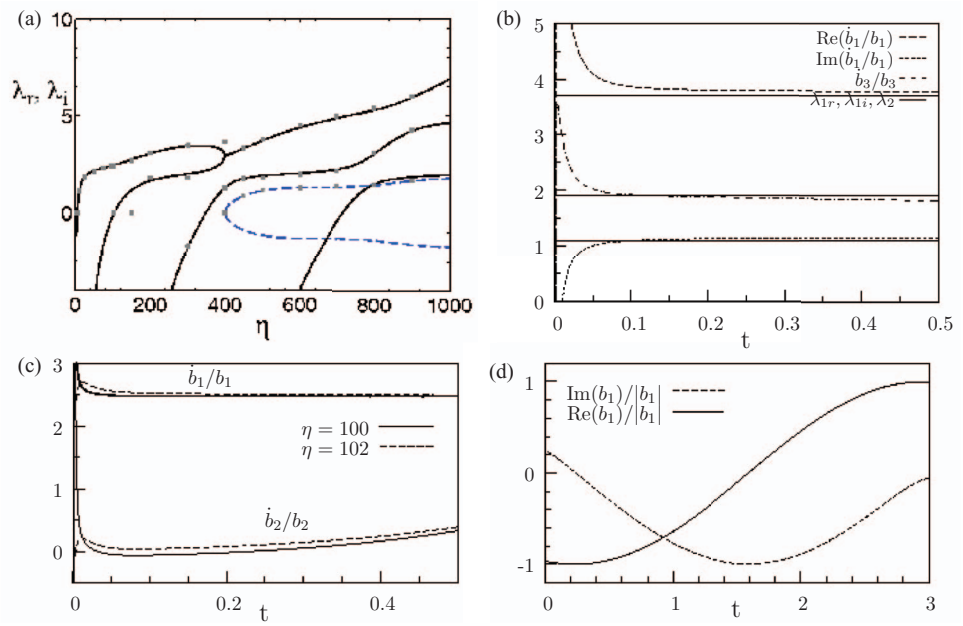

FIG. 6. Comparison between results from linear stability analysis and numerical simulations, for a clamped filament in the flows $\mathbf{U}^\infty = (x, -y)$. (a) The behavior of the first four eigenvalues for increasing η, where lines refer to linear stability (continuous lines for the eigenvalue's real part, dashed lines for the eigenvalue's imaginary part) and markers represent numerical results. (b) For $\eta = 500$ comparison with corresponding ratios $b_i^{-1} db_i/dt$ for a pair of complex conjugate eigenvalues λ_1, λ_1^* and unstable real eigenvalue λ_2. (c) For two values of η slightly smaller and larger than the critical value of η for buckling ($\eta = 100$ and 102) functions $b_1^{-1} db_1/dt$ and $b_2^{-1} db_2/dt$ versus time. (d) For $\eta = 500$, we plot versus time the real and the imaginary part of the coefficient b_1, associated with the complex eigenfunction ϕ_1, divided by the modulus of b_1.

here are characterized by a non-Hermitian matrix and the associated basis is non-orthonormal. Such an expansion allows us to directly compare results from linear stability and numerical simulations (Figure 6(a), for the case of a clamped filament in a linear flow). We find good agreement between the two approaches for all the configurations considered. Figure 6(c) shows the behavior of the ratios $b_1^{-1} db_1/dt$ and $b_2^{-1} db_2/dt$ as a function of time for two values of η chosen slightly smaller and larger than the critical value of η for buckling ($\eta = 100$ and 102 for a clamped filament in a linear flow). We note that while $b_1^{-1} db_1/dt$ remains constant during the transient and equal to the value of λ_1 as found from linear stability, $b_2^{-1} db_2/dt$ grows with time and at the beginning of the transient displays a minimum which matches the value of λ_2 (in this case $\lambda_2 \approx 0$ since we chose values of η very close to η_{c2}). In Figure 6(b), we compare the values of the two unstable eigenvalues predicted by linear theory for $\eta = 500$ with the corresponding ratios $b_i^{-1} db_i/dt$ as obtained from numerical simulations. In this case, note that the eigenvalues with largest real part are complex conjugate (see also Fig. 6(a)) and the comparison is shown for both the real and the imaginary part.

D. Standing waves

As indicated in Sec. IV B, the solution for a tethered filament, either hinged or clamped, in an extensional flow is characterized by the presence, for η large enough, of pairs of complex conjugate eigenvalues and eigenvectors. In Figure 6(a), we show the real and imaginary parts of the eigenvalues of largest real part for a clamped filament in a linear extensional flow as function of η. We observe that at $\eta = 400$ a pair of complex conjugate eigenvalues appear, with associated complex conjugate eigenfunctions. Indeed more pairs of complex conjugate eigenvalues appear for values of η larger than shown in the graph. We can show that the portion of the solution $x_1(s, t)$ that corresponds to a pair of complex conjugates eigenvalues is characterized by two waveforms that oscillate in time and

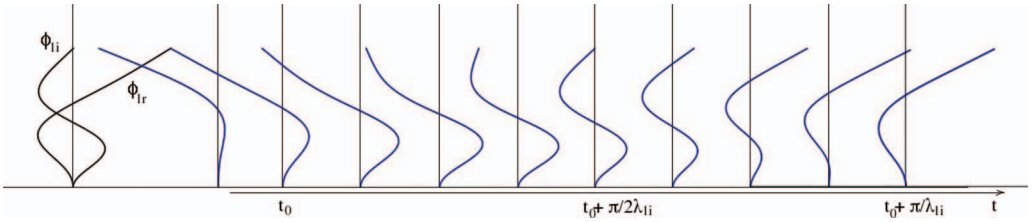

FIG. 7. On the left of the plot, the real and imaginary component of the first eigenvector, ϕ_{1r} and $\phi_{1\iota}$, are shown. Along the axis t the evolution of the filament with time, where the position of the beam x_1 has been divided by the exponentially growing part of the solution, $\exp(\lambda_{1r}t)$.

is enveloped in an exponentially growing function. For example, for $\eta = 500$ we have

$$\begin{aligned} x_1 &\simeq e^{(\lambda_1 t)}\phi_1 + e^{(\lambda_1^* t)}\phi_1^* + e^{(\lambda_3 t)}\phi_3 + ... \\ &\simeq 2e^{(\lambda_{1r} t)}(\phi_{1r}\cos\lambda_{1\iota} t - \phi_{1\iota}\sin\lambda_{1\iota} t) + e^{(\lambda_3 t)}\phi_3 + ..., \end{aligned} \tag{10}$$

where ϕ_{1r} and $\phi_{1\iota}$ are, respectively, the real and the imaginary part of the complex eigenvector ϕ_1, which is associated with the eigenvalue $\lambda_1 = \lambda_{1r} + \imath\lambda_{1\iota}$, and λ_1^* and ϕ_1^* are complex conjugates of, respectively, λ_1 and ϕ_1. The two waveforms ϕ_{1r} and $\phi_{1\iota}$ oscillate in time with a frequency $\lambda_{1\iota}/(2\pi)$ and grow exponentially at a rate λ_{1r}. In Figure 7, the numerically calculated nonlinear evolution of the filament at various instants during the transient is shown, where the solution for the filament position x_1 has been divided by $\exp(\lambda_{1r}t)$. Moreover, on the left of the plot the two eigenfunctions ϕ_{1r} and $\phi_{1\iota}$ are displayed for reference. It is easy to see that the shape of the filament at $t = t_0 \simeq 0.2$ is very close to the shape of $-\phi_{1r}$; later at $t = t_0 + 0.5\pi/\lambda_{1\iota}$ this first mode has disappeared and the shape of the filament has evolved into $\phi_{1\iota}$. After another quarter of period the shape of the filament has evolved to ϕ_{1r}. As a further clarification, we plot in Figure 6(d) the real and the imaginary parts of the projection of the filament shape on the eigenfunction ϕ_1 (divided by its norm) as a function of time. These quantities are proportional to the amplitude of the two waveforms, as shown in Eq. (10), and clearly behave as $\cos(\lambda_{1\iota}t)$ and $\sin(\lambda_{1\iota}t)$.

V. WEAKLY NONLINEAR THEORY

We would like to understand how nonlinearities modify the behavior of the described dynamical system. It is known in fact that after some time the nonlinear self-interactions of the dominant mode in proximity of critical points generates harmonics that may moderate or accelerate the exponential growth of the linear disturbance predicted by linear theory. This behavior is described by the so-called Landau equation, which provides the time evolution of the amplitude A of the dominant mode.[28]

Hence, we take as "base" solution for the filament, identified by the superscript 0, the position $x_i^0 = s\delta_{i2}$, which also corresponds to the velocity distribution $U_i^0 = U_i^\infty(x_i^0)$ and the tension distribution T^0, obtained for the "base" state from Eq. (1). We introduce the "perturbed" state variables $\tilde{x}_i = x_i - x_i^0$, $\tilde{U}_i = U_i^\infty - U_i^0$ and $\tilde{T} = T - T^0$. From Eq. (1) and the inextensibility constrain $x_{i,s}x_{i,s} = 1$ we can derive a new set of governing equations in terms of the perturbed state variables, which will be completed by the boundary conditions $\tilde{x}_{i,ss} = \tilde{x}_{i,sss} = 0$ for $s = 1$ and either $\tilde{x}_i = \tilde{x}_{i,s} = 0$ (clamped filament) or $\tilde{x}_i = \tilde{x}_{i,ss} = 0$ (hinged filament) for $s = 0$ (see Appendix A, Eq. (A1)).

We examine the nonlinear instability when the flow is "weakly" unstable, that is, for $(\eta - \eta_{c1}) \ll 1$, when all the normal modes except the first one decay exponentially in time, so that they can be neglected, and the first mode grows very slowly in time (the associated eigenvalue λ_1 is very small). However small the disturbance A_0 will be initially, it will cease to be small by a time of order $O(\log A_0/\lambda_1) \approx (\log A_0)/(\eta - \eta_{c1})$ as $\eta \to \eta_{c1}$, by which time nonlinearities will have modified the exponential growth. Hence, we expand the "perturbed" variables describing the position of the filament and the tension in the filament as

$$\tilde{x}_i = (u^1 + u^2 + u^3 + ...)\delta_{i1} + (v^1 + v^2 + v^3 + ...)\delta_{i2}\,, \tag{11}$$

$$\tilde{T} = T^1 + T^2 + T^3 + \dots , \tag{12}$$

where

$$u^1 = A(t)\phi(s,\eta) \quad \text{with} \quad L(\phi(s),\eta) = \lambda\phi(s) , \tag{13}$$
$$\phi_{,ss} = \phi_{,sss} = 0 \ \text{ at } \ s = 1 , \ \phi = \phi_{,s} = 0 \ \text{ or } \ \phi = \phi_{,ss} = 0 \ \text{ at } \ s = 0 ,$$

and

$$u^r \sim O(A^r) , \quad v^{r-1} \sim O(A^r) , \quad r = 2, 3, \dots . \tag{14}$$

Note that the superscripts on the variables u, v, and T refer to the order of the expansion, whereas the superscripts on A refer to the power of the amplitude. These are related via Eq. (14). We seek the coefficients a_1, a_2, a_3 which appear in the equation for the amplitude $A(t)$,

$$\frac{dA}{dt} = a_1 A + a_2 A^2 + a_3 A^3 + \dots . \tag{15}$$

By substituting the expansions into the governing equations, we find at first order that $T^1 = 0$ and $a_1 = \lambda(\eta)$. At second order we have

$$v^1 = -A^2 f(s,\eta) \ \text{ and } \ T^2 = -A^2 g(s,\eta) , \tag{16}$$

where $f(s, \eta)$ and $g(s, \eta)$ are expressed in terms of the known $\phi(s, \eta)$, and $u^2 = 0$, $a_2 = 0$. Finally, at third order, by computing the inner product of Eq. (A1) with $\phi^\dagger(s, \eta)$ (the solution of the adjoint linear problem $L^\dagger(\phi^\dagger(s), \eta)$), we obtain an expression for a_3 in term of $\phi(s, \eta)$, $\phi^\dagger(s, \eta)$, $f(s, \eta)$, $g(s, \eta)$.

We are then able to evaluate the coefficients a_1 and a_3 of the Landau equation for the specific flow configuration and boundary conditions and for the various critical points. More details about the derivation that we summarize here are provided in Appendix A, as well as the numerical expressions for the Landau equation.

We find that, for both the linear and the quadratic extensional flows and the two boundary conditions at the base, the filament always presents supercritical stability (a_3 in Eq. (15) is negative) for all the critical points listed in Table I. Note that for each critical point we assume only one unstable mode to be present and equal to the mode experiencing marginal stability. In Figure 8, the behavior of a clamped filament in proximity to the bending critical point ($\eta - \eta_{c1} \ll 1$) for the two flow configurations is presented. In both cases, we plot as function of time the quantity $A^{-1}dA/dt$ when the "base" state configuration is perturbed at time $t = 0$ with $u^1 = A_0\phi(s, \eta)$, for various A_0. Moreover, we compare the results obtained via numerical simulations using the bead-rod model with results predicted by the Landau equation for the same initial conditions. We observe that $A^{-1}dA/dt$ is a decreasing function of time and it is smaller for larger initial perturbations. This implies that

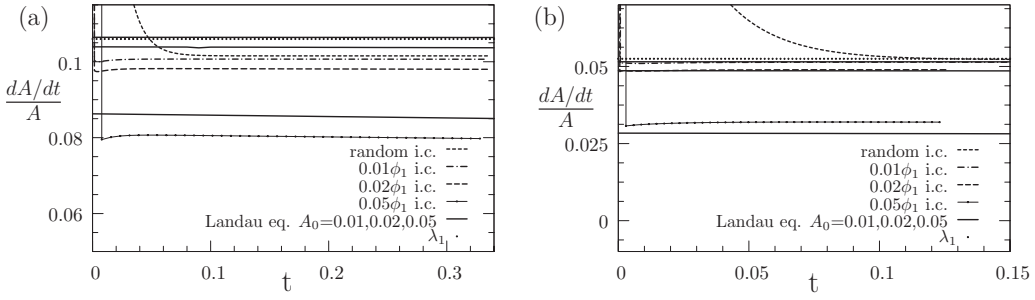

FIG. 8. Behavior of a filament (a) in a linear extensional flow and (b) in a quadratic extensional flow when an initial perturbation is applied and for a value of $\eta = \eta_c + \Delta\eta$, with $\Delta\eta/\eta \simeq \epsilon^2$, $\epsilon = 0.2$ and η_c the critical point for bending. The ratio $A^{-1}dA/dt$ is plotted versus time for a Gaussian small initial perturbation and for a perturbation $u^1 = A_0\phi(s, t)$, with ϕ the unstable eigenvector and various $A_0 = 0.01$, 0.02, 0.05, as obtained from bead-rod model simulations and from the integration of the Landau equation (continuous lines for various A_0).

for values of η larger than η_c an initial perturbation will grow at a speed lower than exponential, while for values of η smaller than η_c, the initial perturbation will always decay. As we can see from Figure 8 the agreement between bead-rod chain numerical simulations and weakly nonlinear theory is satisfactory. Consistent with these findings, preliminary results from numerical simulations shows that the addition of thermal fluctuations does not destabilize the behavior of the elastic filament for values of the effective compliance close to the critical values. In fact, we see that thermal fluctuations have the effect of relaxing a compressed filament, thus delaying its buckling dynamics and collapse, as already explained in Ref. 16.

VI. CONCLUSION

We have developed a linear stability analysis for an elastic inextensible filament tethered at its base in two distinct two-dimensional extensional flows. The filament is initially aligned with the compression axis of the flow. We identify the critical values of the dimensionless compliance η that leads to bending and buckling instabilities, for both a linear extensional flow and a wall stagnation point flow. Also, we perform numerical simulations of the complete nonlinear problem using an appropriate discrete chain model. Finally, we develop a weakly nonlinear analysis, leading to an amplitude equation which shows supercritical stability for the bending and buckling transitions in both flows. There is a good agreement between the various analysis and numerical simulations.

ACKNOWLEDGMENTS

We would like to thank Nicolas Autrusson, with whom the authors initially collaborated on this subject when he was visiting Princeton University.

APPENDIX A: LANDAU EQUATION

We introduce a set of variables that characterize the "perturbed" state and are related to the variables of our problem and the "base" state variables by the relations $x_i = \tilde{x}_i + x_i^0$, $U_i^\infty = \tilde{U}_i + U_i^0$ and $T = \tilde{T} + T^0$. If we replace these definitions in the governing equation for the filament dynamics, Eq. (1), for the case $\mathbf{U}^\infty = (x, y)$, we obtained an equation for the "perturbed" state that reads

$$2\tilde{U}_i + s\tilde{x}_{i,s} + \delta_{i2}(s\tilde{x}_{2,s} - \tilde{U}_2 - \tilde{x}_{j,s}\tilde{U}_j) + s\tilde{x}_{i,s}\tilde{x}_{2,s} - \tilde{U}_2\tilde{x}_{i,s} - \tilde{x}_{i,s}\tilde{x}_{j,s}\tilde{U}_j =$$

$$2\tilde{x}_{i,t} - (\delta_{i2} + \tilde{x}_{i,s})(\tilde{x}_{2,t} + \tilde{x}_{j,s}\tilde{x}_{j,t}) - s\tilde{x}_{i,s} - \frac{s^2-1}{2}\tilde{x}_{i,ss} + \frac{2}{\eta_c}\left(\tilde{x}_{i,ssss} - (\delta_{i2} + \tilde{x}_{i,s})\tilde{T}_s - \tilde{T}\tilde{x}_{i,ss}\right)$$

$$+\frac{2(\eta_c - \eta)}{\eta_c \eta}\left(\tilde{x}_{i,ssss} - (\delta_{i2} + \tilde{x}_{i,s})\tilde{T}_s - \tilde{T}\tilde{x}_{i,ss}\right) \quad \text{for } i = 1, 2. \tag{A1}$$

Moreover, the problem is closed by the inextensibility condition

$$2\tilde{x}_{2,s} + \tilde{x}_{i,s}\tilde{x}_{i,s} = 0\,, \tag{A2}$$

and by the boundary conditions $\tilde{x}_{i,ss} = \tilde{x}_{i,sss} = 0$, $\tilde{T} = 0$ at the free end ($s = 1$), $\tilde{x}_i = \tilde{x}_{i,s} = 0$ or $\tilde{x}_i = \tilde{x}_{i,ss} = 0$ at the base ($s = 0$). The "perturbed" variables $\tilde{x}_i$ and $\tilde{T}_i$ are then expanded according to (11)–(14). At first order, Eq. (A1) reduces along coordinate "1" to

$$u^1 + su_s^1 + \frac{(s^1 - 1)}{4}u_{ss}^1 - \frac{u_{ssss}^1}{\eta} = u_t^1, \tag{A3}$$

which for $u^1 = A(t)\phi(s, \eta)$ provides $a_1 = \lambda(\eta)$, and along coordinate "2" to $T^1 = 0$. Further, from the inextensibility condition (A2) we obtain

$$v^1 = -A^2 f(s, \eta) = -\frac{A^2}{2}\int_0^s \phi_s^2(s, \eta)ds\,. \tag{A4}$$

At second order for coordinate "1" we obtain an equation in u^2 similar to (A3) and that is only solvable for $a_2 = 0$ and $u^2 = 0$, while for coordinate "2" the following equation holds:

$$\eta(-\frac{v^1}{2} + \frac{3}{2}sv_s^1 + \frac{(s^2-1)}{4}v_{ss}^1 - u^1u_s^1) - v_{ssss}^1 + T_s^2 = 0, \tag{A5}$$

and provides an integrable expression for T^2

$$T^2 = -A^2g(s,\eta) = -\int_s^1 v_{ssss}^1 + \frac{\eta}{2}\left[v^1 - 3sv_s^1 + u^1u_s^1 - \frac{s^2-1}{2}v_{ss}^1\right]. \tag{A6}$$

Finally, Eq. (A1) evaluated at third order along coordinate "1" provides

$$u^3 + su_s^3 + \frac{(s^2-1)}{4}u_{ss}^3 - \frac{u_{ssss}^3}{\eta} + \frac{1}{\eta}(T^2u_s^1)_s + \tag{A7}$$

$$\frac{1}{2}(v^1u_s^1 + sv_s^1u_s^1 - u^1(u_s^1)^2) = a_3A^3\phi(s,\eta);$$

by performing an inner product with $\phi^\dagger(s,\eta)$, eigenvector of the adjoint problem, we obtain

$$a_3 = -\frac{\langle s\phi_s f_s, \phi^\dagger\rangle + \langle \phi_s f, \phi^\dagger\rangle + \langle \phi\phi_s^2, \phi^\dagger\rangle + 2\langle(\phi_s g)_s, \phi^\dagger\rangle/\eta}{\langle\phi, \phi^\dagger\rangle}. \tag{A8}$$

It is possible in this way to evaluate the coefficients of the Landau equation for the specific case, once the eigenvectors $\phi(\eta)$ and $\phi^\dagger(\eta)$ for the linear problems $L(\phi(s), \eta) = \lambda\phi(s)$ and $L^\dagger(\phi^\dagger(s), \eta) = \sigma\phi^\dagger(s)$ are known.

For the flow configuration $\mathbf{U}^\infty = (x, y)$, we have

$$L(\phi) = \phi + s\phi_s + (s^2-1)\frac{\phi_{ss}}{4} - \frac{1}{\eta}\phi_{ssss} = \lambda\phi, \tag{A9}$$

$$L^\dagger(\phi^\dagger) = \phi^\dagger + (s^2-1)\frac{\phi_{ss}^\dagger}{4} - \frac{1}{\eta}\phi_{ssss}^\dagger = \sigma\phi^\dagger, \tag{A10}$$

with

$$B(\phi) = \{\phi(0) = 0, \phi_s(0) = 0, \phi_{ss}(1) = 0, \phi_{sss}(1) = 0\},$$
$$B^\dagger(\phi) = \{\phi^\dagger(0) = 0, \phi_s^\dagger(0) = 0, \phi_{ss}^\dagger(1) = 0, (\phi_{sss}^\dagger/\eta + \phi^\dagger/2)(1) = 0\}$$

or

$$B(\phi) = \{\phi(0) = 0, \phi_{ss}(0) = 0, \phi_{ss}(1) = 0, \phi_{sss}(1) = 0\},$$
$$B^\dagger(\phi^\dagger) = \{\phi^\dagger(0) = 0, (\phi_{ss}^\dagger/\eta + \phi^\dagger/4)(0) = 0, \phi_{ss}^\dagger(1) = 0, (\phi_{sss}^\dagger/\eta + \phi^\dagger/2)(1) = 0\}.$$

For the flow configuration $\mathbf{U}^\infty = (xy, -y^2/2)$, we have

$$L(\phi) = s\phi + \frac{s^2}{2}\phi_s + (s^3-1)\frac{\phi_{ss}}{12} - \frac{1}{\eta}\phi_{ssss} = \lambda\phi, \tag{A11}$$

$$L^\dagger(\phi^\dagger) = \frac{s}{2}\phi^\dagger + (s^3-1)\frac{\phi_{ss}^\dagger}{12} - \frac{1}{\eta}\phi_{ssss}^\dagger = \sigma\phi^\dagger, \tag{A12}$$

with

$$B(\phi) = \{\phi(0) = 0, \phi_s(0) = 0, \phi_{ss}(1) = 0, \phi_{sss}(1) = 0\},$$
$$B^\dagger(\phi) = \{\phi^\dagger(0) = 0, \phi_s^\dagger(0) = 0, \phi_{ss}^\dagger(1) = 0, (\phi_{sss}^\dagger/\eta + \phi^\dagger/4)(1) = 0\}$$

or

$$B(\phi) = \{\phi(0) = 0, \phi_{ss}(0) = 0, \phi_{ss}(1) = 0, \phi_{sss}(1) = 0\},$$
$$B^\dagger(\phi^\dagger) = \{\phi^\dagger(0) = 0, (\phi_{ss}^\dagger/\eta + \phi^\dagger/4)(0) = 0, \phi_{ss}^\dagger(1) = 0, (\phi_{sss}^\dagger/\eta + \phi^\dagger/4)(1) = 0\}.$$

Finally, we list here the particular form of the Landau equation for a clamped filament in the flow field $\mathbf{U}^\infty = (x, y)$ for η close to $\eta_{c1} = 5.25$

$$\frac{dA}{dt} = 0.1A - 8.4A^3 \quad \text{for} \quad \eta = \eta_{c1} + 0.24, \tag{A13}$$

and to $\eta_{c2} = 103.7$

$$\frac{dA}{dt} = 0.17A - 10.2A^3 \quad \text{for} \quad \eta = \eta_{c2} + 4.3, \tag{A14}$$

in the flow field $\mathbf{U}^\infty = (xy, -y^2/2)$ at $\eta_{c1} = 9.13$

$$\frac{dA}{dt} = 0.05A - 8.6A^3 \quad \text{for} \quad \eta = \eta_{c1} + 0.37, \tag{A15}$$

and to $\eta_{c2} = 250$

$$\frac{dA}{dt} = 0.06A - 14.4A^3 \quad \text{for} \quad \eta = \eta_{c2} + 10. \tag{A16}$$

For a hinged filament in the flow field $\mathbf{U}^\infty = (x, y)$ for η close to $\eta_{c1} = 48.4$ the Landau equation reads

$$\frac{dA}{dt} = 0.2A - 17.2A^3 \quad \text{for} \quad \eta = \eta_{c1} + 2.2, \tag{A17}$$

in the flow field $\mathbf{U}^\infty = (xy, -y^2/2)$ at $\eta_{c1} = 122.6$

$$\frac{dA}{dt} = 0.06A - 16.5A^3 \quad \text{for} \quad \eta = \eta_{c2} + 5.4. \tag{A18}$$

APPENDIX B: BEAD-WALL INTERACTION FORCE

The wall exclusion force is modeled using a bead-wall repulsive potential which accounts for the Lennard-Jones contribution, as proposed by Hoda and Kumar[26]

$$\begin{aligned} F_i^W &= 4\pi\epsilon_w d_{ev}\left(\left(\frac{d_{ev}}{2r_c}\right)^{11} - \left(\frac{d_{ev}}{2r_c}\right)^{5}\right)\mathbf{e}_2 \quad \text{for} \quad y_i \le r_c \\ &= 4\pi\epsilon_w d_{ev}\left(\left(\frac{d_{ev}}{2y_i}\right)^{11} - \left(\frac{d_{ev}}{2y_i}\right)^{5}\right)\mathbf{e}_2 \quad \text{for} \quad r_c < y_i < 0.5 \\ &= 0 \quad \text{for} \quad y_i \ge 0.5, \end{aligned}$$

where ϵ_w, d_{ev}, r_c are adjustable parameters that we chose for our simulations as $\epsilon_w = 1, d_{ev} = 0.8, r_c = 0.3$.

[1] R. E. Goldstein and S. A. Langer, "Nonlinear dynamics of stiff polymers," Phys. Rev. Lett. **75**, 1094–1097 (1995).
[2] C. H. Wiggins, D. Riveline, A. Ott, and R. E. Goldstein, "Trapping and wiggling: Elastohydrodynamics of driven microfilaments," Biophys. J. **74**, 1043–1060 (1998).
[3] S. A. Koehler and T. R. Powers, "Twirling elastica: Kinks, viscous drag, and torsional stress," Phys. Rev. Lett. **85**, 4827–4830 (2000).
[4] N. Coq, O. du Roure, J. Marthelot, D. Bartolo, and H. Fermigier, "Rotational dynamics of a soft filament: Wrapping transition and propulsive forces," Phys. Fluids **20**, 051703 (2008).
[5] D. J. Smith, E. Gaffney, and J. Blake, "Modelling mucociliary clearance," Respir. Physiol. Neurobiol. **163**, 178–188 (2008).
[6] D. J. Smith, J. R. Blake, and E. A. Gaffney, "Fluid mechanics of nodal flow due to embryonic primary cilia," J. R. Soc. Interface. **5**, 567–573 (2008).
[7] J. H. E. Cartwright, N. O. Piro, and I. Tuval, "Embryonic nodal flow and the dynamics of nodal vesicular parcels," J. R. Soc., Interface **4**, 49–55 (2007).
[8] L. J. Fauci and R. Dillon, "Biofluidmechanics of reproduction," Annu. Rev. Fluid Mech. **38**, 371–394 (2006).
[9] R. Rusconi, S. Lecuyer, L. Guglielmini, and H. A. Stone, "Laminar flow around corners triggers the formation of biofilm streamers," J. R. Soc., Interface **7**, 1293–1299 (2010).

[10] R. Rusconi, N. Autrusson, L. Guglielmini, S. Lecuyer, and H. A. Stone, "Secondary flow as a mechanism for biofilm streamers formation," Biophys. J. **100**, 1392–1399 (2011).
[11] S. Kharchenko, J. Douglas, J. Obrzut, E. Grulke, and K. Migler, "Fluid mechanics of nodal flow due to embryonic primary cilia," Nature Mater. **3**, 564–568 (2003).
[12] M. A. Zirnsak, D. U. Hur, and D. Boger, "Normal stresses in fibre suspensions," J. Non-Newtonian Fluid Mech. **54**, 153–193 (1994).
[13] L. Becker and M. Shelley, "Instability of elastic filaments in shear flow yields first-normal stress differences," Phys. Rev. Lett. **87**(19), 198301 (2001).
[14] Y.-N. Young and M. Shelley, "Stretch-coil transition and transport of fibers in cellulars flows," Phys. Rev. Lett. **99**, 058303 (2007).
[15] E. Wandersman, N. Quennouz, M. Fermigier, A. Lindner, and O. du Roure, "Buckled in translation," Soft Matter **6**, 5715–5719 (2010).
[16] K. Baczynski, R. Lipowsky, and J. Kierfeld, "Stretching of buckled filaments by thermal fluctuations," Phys. Rev. E **76**, 061914 (2007).
[17] C. Pozrikidis, "Shear flow past slender elastic rods attached to a plane," Int. J. Solids Struct. **48**, 137–143 (2011).
[18] N. Autrusson, L. Guglielmini, S. Lecuyer, R. Rusconi, and H. A. Stone, "The shape of an elastic filament in a two-dimensional corner flow," Phys. Fluids **23**, 99–99 (2011).
[19] V. Beck and A. Shaqfeh, "Ergodicity breaking and conformal hysteresis in the dynamics of a polymer tethered at a surface stagnation point," J. Chem. Phys. **124**, 094902 (2006).
[20] R. G. Cox, "The motion of long slender bodies in a viscous fluid. Part 1. General theory," J. Fluid Mech. **44**, 791–810 (1970).
[21] H. A. Kramers, *Collected Scientific Papers* (North-Holland, Amsterdam, 1956).
[22] O. Kratky and G. Porod, "Rontgenuntersuchung geloster fadenmolekule," Recl. Trav. Chim. Pays-Bas **68**, 1106 (1949).
[23] C. A. Lueth and E. G. Shaqfeh, "Tethered dna shear dynamics in the flow gradient plane: Application to double tethering," Korea-Aust. Rheol. J. **19**, 141–146 (2007).
[24] H. C. Ottinger, *Stochastic Processes in Polymer Fluids* (Springer, Berlin, 1996).
[25] R. A. Harris and J. E. Hearst, "On polymer dynamics," J. Chem. Phys. **44**, 2595–2602 (1966).
[26] N. Hoda and S. Kumar, "Brownian dynamics simulations of polyelectrolyte adsorption in shear flow with hydrodynamic interaction," J. Chem. Phys. **127**, 234902 (2007).
[27] M. Somasi, B. Khomani, N. J. Woo, J. S. Hur, and E. Shaqfeh, "Brownian dynamics simulations of bead-rod and bead-spring chains: Numerical algorithms and coarse-graining issues," J. Non-Newtonian Fluid Mech. **108**, 227–255 (2002).
[28] P. G. Drazin and W. H. Reid, *Hydrodynamic Stability* (Cambridge University Press, Cambridge, 2004).